

Received November 16, 2017, accepted December 19, 2017, date of publication January 4, 2018, date of current version February 14, 2018.

Digital Object Identifier 10.1109/ACCESS.2017.2787567

Design of RBFN Controller Based Boost Type Vienna Rectifier for Grid-Tied Wind Energy Conversion System

DAMODHAR REDDY AND SUDHA RAMASAMY^{ID}

School of Electrical Engineering, VIT University, Vellore 632014, India

Corresponding author: Sudha Ramasamy (sudha.r@vit.ac.in)

ABSTRACT This paper presents a radial basis function network (RBFN) controller-based three-phase boost-type Vienna rectifier for a grid-tied wind energy conversion system. Boost-type Vienna rectifier is an ac/dc converter characterized by high power density and improved power factor in addition to maintaining a sinusoidal current with low total harmonic distortion at the input side. Such converter systems find its utility and application related to unidirectional power flow, such as data centers, telecommunication systems, and more appropriately for wind energy conversion systems. This paper involves the implementation of an RBFN-based control strategy for Vienna rectifier to ascertain the ability of the proposed strategy to obtain enhanced performance of a wind energy conversion system. The choice of the RBFN for the control of the rectifier system stems from its inherent capability to ensure better dynamic control notwithstanding its capability to reduce the design complexities during the network training phase. Simulation is carried out using MATLAB Simulink for a 1-kW standalone and grid-tied wind energy conversion system. This paper involves carrying out the detailed analysis and results for different wind velocities under standalone and grid-tied conditions.

INDEX TERMS Wind energy conversion system (WECS), PMSG (permanent magnet synchronous generator), Vienna rectifier, RBFN, DC-link voltage and grid side inverter (GSI).

I. INTRODUCTION

In recent years, due to growing power demand, wind conversion systems are used for small and medium scale energy generation. With advancements in wind turbine design and cost-effective installation of wind farms, the contribution of wind power generation to global energy generation has increased rapidly [1]. According to the Global Wind Energy Council (GWEC), 12.5% (486.8GW) of power production worldwide is based on wind energy systems and a total capacity of 54.6 GW based on wind systems have been installed in 2016 alone. Detailed research studies indicate that Permanent Magnet Synchronous Generator (PMSG) [2], [3] based wind turbine systems are suitable configurations for small-scale islanded wind farm installation [4]. The PMSGs have high efficiency, low operating speed, less weight (due to the absence of field winding and gearbox) and low copper losses. The PMSG has the capability [5] to handle a wide range of rotor speeds with reference to rapidly changing wind velocities. The frequency and output voltage magnitude of the PMSG are varied according to variations in the input

wind velocity. The optimization of load voltage under variable input voltage magnitude and frequency of WECS is obtained utilizing the space vector modulation (SVM) [6] technique. Similarly, research studies have also been proposed in the context of fixed switching frequency and reduced flux and torque ripples [7], utilizing the direct torque control (DTC) of wind energy system.

The Maximum Power Point Tracking (MPPT) is possible in variable speed wind turbine systems through different MPPT techniques [8], [9] like Incremental Conductance, Perturbation and Observation (P&O), Fuzzy Logic control and Artificial Intelligence Control method etc [10], [11]. In this context, it is worth mentioning that Artificial Neural Network (ANN) based controller [12]–[14] has a fast dynamic response, less complex design, ease of input training, good generalization capability etc. Distributed Energy Resources (DERs) are also used extensively due to enormous advancements in power electronic converters.

From the perspective of converter topologies, many AC/DC converter systems are proposed by researchers based

on applications such as diode bridge rectifiers, six-pulse controlled bridge rectifiers and three-level Neutral Point Clamped (NPC) rectifiers etc. Such rectifiers have higher switching losses. Further, it is to be noted that with the increase in the number of switches in the circuit the input current harmonic distortions produced by active semiconductor power switches also increases. To overcome these issues, a unidirectional power flow converter is essential. A three-phase Vienna Rectifier with inherent voltage boosting capability is a better alternative to rectify and to regulate the supply voltage of WECS and the input side ripples are minimized [15], [16] by appropriate inductive-capacitive (LC) and/or EMI (electromagnetic interference) filters. The voltage and current control may be achieved utilizing robust control methods such as feedback linearization and sliding mode in the grid-tied wind energy system [17].

It is also worth noting in this context that high altitude small-scale wind energy conversion systems are proposed based on Vienna rectifier for the distributed loads under variable voltage and frequency conditions [18], [19]. Basically, the Vienna Rectifier [20], [21] provides high power density, reduced harmonics, low switching losses, sinusoidal input current and improved power factor. A three-phase Vienna rectifier approach becomes appropriate when a unidirectional power flow is mandatory. The Vienna Rectifier proposed by J.W. Kolar (1993) is widely used in wind energy conversion systems, telecommunication, data centers and DC distribution systems etc. The boost type Vienna Rectifier is a popularly known three-phase/three-level Pulse Width Modulation (PWM) converter which can be used for single stage energy conversion in the wind turbine systems.

Appropriate control strategies of Vienna rectifier are essential for obtaining improved dynamic performance of the proposed system. Many control topologies [22]–[24] have been proposed by researchers for converter control with balanced DC-link voltage [25] such as Space Vector Pulse Width Modulation (SVPWM) [26], [27], Hysteresis Current Control (HCC) [28] and Model Predictive Control (MPC) [29] etc. However, the complexity of such control structures is comparatively higher with that of intelligent control structures. On the other hand, IGBT (Insulated Gate Bipolar Transistor) based grid side inverters are employed for DC to AC conversion at the DC link and regulate voltage and frequency [30] of the grid. The PWM control technique is used with a suitable switching pattern to control the grid side parameters in a wind-solar based hybrid system [31], [32]. It is hence evident that advanced intelligent controllers are credible alternatives for obtaining a robust system operation with improved efficiency, enhanced input power factor and dc-link voltage control.

Due to the fast convergence and the simple structure of such intelligent control algorithms, an intelligent controller plays a vital role and augurs well as compared to the conventional control structures. In this research study, the design of an RBFN controller based boost type Vienna Rectifier is taken up for implementation, simulated and detailed analysis

for a grid-tied wind energy conversion system working under standalone and grid-tied condition.

II. DESIGN AND ANALYSIS OF PROPOSED SYSTEM

The proposed system consists of four modules namely modeling of a wind turbine for variable wind speed, modeling of PMSG, analysis of AC to DC Vienna Rectifier and DC to AC grid side inverter. Figure 1 depicts the generic layout of the grid-tied wind energy conversion system. Wind turbine system is directly coupled to the PMSG through a shaft at which the wind energy from the wind turbine system is transformed into mechanical energy. It is in turn fed to PMSG where the mechanical energy is transformed into electrical energy. The PMSG output is fed to the source side PWM converter (Vienna Rectifier) where the generated AC is directly converted into DC in a single stage. Further, the voltage appearing at the DC-link is fed to the PWM inverter which can be supplied to supply the load or can be fed to the grid.

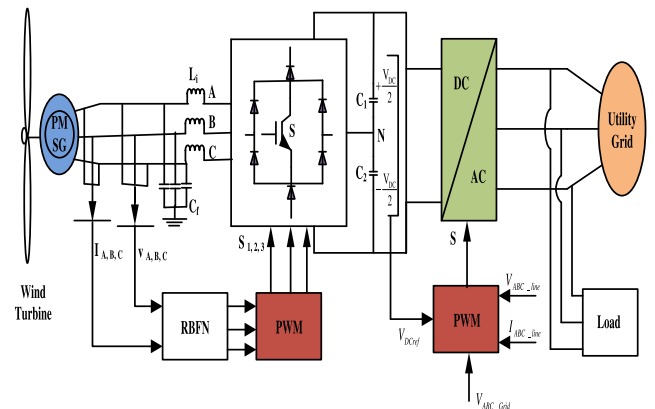


FIGURE 1. Block diagram of a grid-tied wind energy conversion system.

The control of Vienna Rectifier with an intelligent controller (RBFN) results in the maximum power extraction from the wind turbine. The grid side inverter not only provides a balanced DC link voltage but also maintains a constant magnitude of AC voltage which is fed to the load and the grid. The mechanical power output characteristics of the wind turbine obtained from MATLAB Simulink for different wind input velocities at zero pitch angles are plotted in Figure 2.

A. WIND TURBINE MODELLING

The kinetic energy is transformed into mechanical energy by the wind turbine for variable wind speeds. The mechanical output torque of the wind turbine is expressed in terms of air density (kg/m^3), sweep area of the turbine blades, pitch angle, wind velocity, power coefficient and tip-speed ratio. The dynamic behavior of the wind turbine depends on the power or torque coefficient and the output of the turbine is estimated from the wind speed. The maximum output of wind turbine depends on the pitch angle (β) and the tip-speed ratio (λ). The mechanical torque (T_m) produced

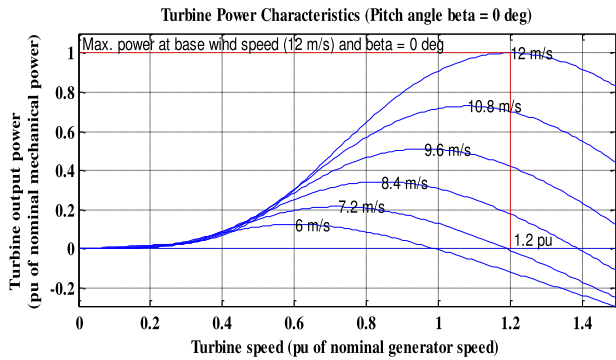


FIGURE 2. Speed vs power characteristics of the wind turbine.

by [2], [3], [8] the wind turbine is expressed as,

$$T_m = \frac{1}{2} \rho A C_p(\lambda, \beta) v^3 \frac{1}{\omega^3} \quad (1)$$

Where, ρ = Air density (kg/m^3), C_p = Power Coefficient, A = Sweep area of turbine blades (m^2), β = Pitch angle (deg), v = Wind speed (m/s), ω = Rotor angular velocity (rad/sec) and λ = Tip-ratio. Then λ can be expressed as

$$\lambda = \frac{\omega_m R}{v} \quad (2)$$

Where R = Rotor radius (m).

Similarly, the mechanical power produced by the wind turbine system is expressed as

$$P_m = \frac{1}{2} \rho A C_p(\lambda, \beta) v^3 \quad (3)$$

B. PMSG MODELLING

The mechanical energy is transformed into electrical energy by the PMSG at low rotor speeds. Output energy is dependent on variable wind input, where the rotor of PMSG is coupled with the turbine shaft. It has the benefits of low rotor inertia, high power density, low copper loss due to the absence of field winding and low cost. The electrical energy (voltage) generated by the PMSG [2], [3], [8] is expressed in the rotor reference frame as,

$$V_{gq} = (R_g + pL_q)i_q + \omega_e(L_d i_d + \psi_f) \quad (4)$$

$$V_{gd} = (R_g + pL_d)i_d - \omega_e L_q i_q \quad (5)$$

Where, i_d , V_{gd} and i_{iq} , V_{gq} are the d - q axis stator current and voltage respectively. L_d and L_q are the d - q axis inductance of generator, ψ_f = Magnetic flux (wb) and R_g refers to the stator winding resistance of the generator (Ω).

ω_e is the electrical speed of the generator. The ω_e is expressed as

$$\omega_e = p_n \omega_m \quad (6)$$

The electromagnetic torque (T_{Elec}) of the PMSG is expressed as,

$$T_{Elec} = \frac{3}{2} [\psi_f i_q - (L_d - L_q) i_d i_q] \quad (7)$$

Therefore, the wind turbine dynamic model equation is expressed as,

$$J \frac{d\omega_m}{dt} = T_{Elec} - T_m - F\omega_m \quad (8)$$

Where J = moment of inertia & F = Viscous friction coefficient.

$$\left. \begin{aligned} E_A &= E_m \sin(\omega t) \\ E_B &= E_m \sin(\omega t - \frac{2\pi}{3}) \\ E_C &= E_m \sin(\omega t + \frac{2\pi}{3}) \end{aligned} \right\} \quad (9)$$

The design parameters considered for wind turbine system simulation are given in Table 1.

TABLE 1. Wind turbine unit parameters.

S. No	Wind system parameters	Ratings
1	Wind base speed	12m/s
2	Pitch angle	0°
3	Torque constant	1.8
4	Flux linkage	1.2Wb-t
5	Stator phase resistance	3.07Ω
6	Armature inductance	6.57mH
7	Maximum voltage at base speed	230V
8	Maximum output power at base speed	1kW

C. VIENNA RECTIFIER (AC/DC PWM CONVERTER)

Vienna rectifier is a unidirectional PFC (power factor correction) rectifier comprising three switches and eighteen diodes as shown in Figure 3. Advantages are sinusoidal input current, balanced output DC-link voltage, low voltage stress across switches, high switching operation and high efficiency. Boost type Vienna rectifier is preferable for wind energy generation, micro-turbines and Low Voltage Direct Current (LVDC) distribution (output voltage levels of 400V-750V-1500V). The current flow in the circuit is dependent on the switching pattern, as mentioned in Table 2.

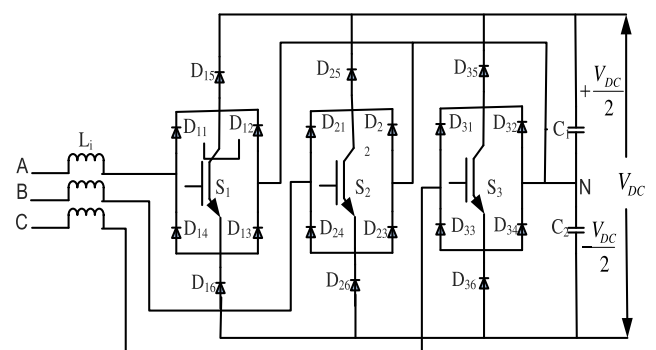


FIGURE 3. Circuit diagram of boost type vienna rectifier.

As shown in Figure 4a & 4b, when $S_1 = 0$ (i.e. switch-OFF), current (Phase-A) flows through the diodes from phase to neutral (for positive I_A) and from neutral to phase (for negative I_A).

TABLE 2. Switching pattern.

S_1	S_2	S_3	V_{AN}	V_{BN}	V_{CN}	Charge	Discharge
0	0	0	$\frac{V_{DC}}{2}$	$\frac{V_{DC}}{2}$	$\frac{V_{DC}}{2}$	C_1, C_2	-
0	0	1	$\frac{V_{DC}}{2}$	$\frac{V_{DC}}{2}$	0	C_1, C_2	-
0	1	0	$\frac{V_{DC}}{2}$	0	$\frac{V_{DC}}{2}$	C_1	C_2
0	1	1	$\frac{V_{DC}}{2}$	0	0	C_1	C_2
1	0	0	0	$\frac{V_{DC}}{2}$	$\frac{V_{DC}}{2}$	C_1, C_2	-
1	0	1	0	$\frac{V_{DC}}{2}$	0	C_2	C_1
1	1	0	0	0	$\frac{V_{DC}}{2}$	C_1	C_2
1	1	1	0	0	0	-	C_1, C_2

Similarly as shown in Figure 4c & 4d, when $S_1 = 1$ (switch-ON) current flows through the switch S_1 from phase to neutral (for positive I_A) and from neutral to phase (for negative I_A).

The state space equations for the input side voltage of rectifier are [17], [20], [21] written as,

$$\left. \begin{aligned} E_A &= R i_A + L \frac{di_A}{dt} + V_{AN} \\ E_B &= R i_B + L \frac{di_B}{dt} + V_{BN} \\ E_C &= R i_C + L \frac{di_C}{dt} + V_{CN} \end{aligned} \right\} \quad (10)$$

Where R is source resistance, L is source inductance and V_{AN} , V_{BN} and V_{CN} are the terminal voltages [17], [20], [21] which can be written as the function of current and state of the switch.

$$\left. \begin{aligned} V_{AN} &= \frac{V_{DC}}{2} \text{sgn}(i_A)(1 - S_1) \\ V_{BN} &= \frac{V_{DC}}{2} \text{sgn}(i_B)(1 - S_2) \\ V_{CN} &= \frac{V_{DC}}{2} \text{sgn}(i_C)(1 - S_3) \end{aligned} \right\} \quad (11)$$

Where, 'sgn' is the signum function of $i_{A,B,C}$ and the output capacitor voltage of the Vienna rectifier which is split into C_1 and C_2 respectively. This voltage control ensures a balanced output and halves DC link voltage across the switches. Therefore, the DC link capacitor voltage is written as,

$$\left. \begin{aligned} V_{DC} &= V_{DC1} + V_{DC2} \\ \Delta V &= V_{DC1} - V_{DC2} \end{aligned} \right\} \quad (12)$$

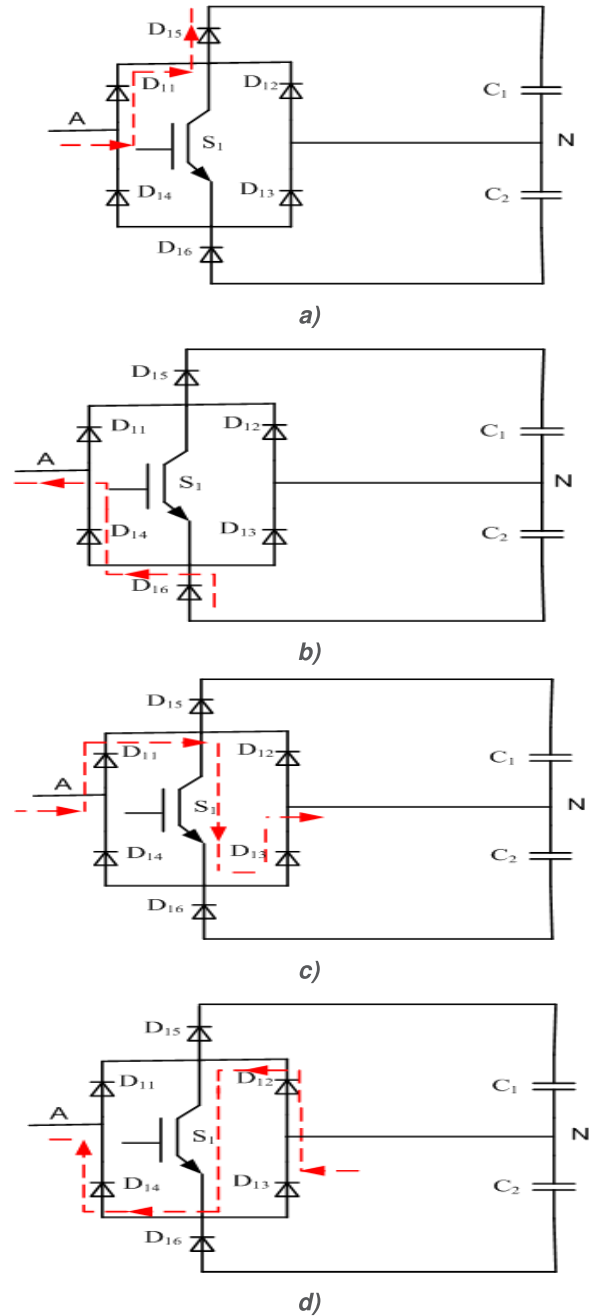


FIGURE 4. Current flow in the circuit when $S_1 = 0$ (Figure.4a: I_A +ve & Figure.4b: I_A -ve) and $S_1 = 1$ (Figure.4c: I_A +ve & Figure.4d: I_A -ve).

Current through the output capacitor is written as,

$$\left. \begin{aligned} i_{C1} &= C_1 \frac{d V_{DC1}}{dt} \\ i_{C2} &= C_2 \frac{d V_{DC2}}{dt} \end{aligned} \right\} \quad (13)$$

The DC link voltages are equally distributed at the output side capacitor to maintain a balanced DC bus voltage.

III. RBFN CONTROLLER

Conventional controllers are limited by controller design complexity, slow dynamic response and high components cost. Hence RBFN based controller is used to obtain faster

dynamic response than that of conventional converter controllers. Though the proposed network is similar to feed-forward network, it has both supervised and unsupervised phases. It has three layers namely input layer, a hidden layer and an output layer. Hidden layer activation functions are estimated from the distance between input and prototype vectors. Firstly, the parameters which direct the basis function are estimated by unsupervised methods. In the next step, the final layer units are decided. The input variable (x_{i1}) to RBFN controller includes voltage and current, and the output variable (y_{k3}) is duty cycle (D). Controller output (as depicted in Figure 5) is given to the Pulse Width Modulation (PWM) pulse generator to generate the switching pattern for Vienna rectifier. The parameters considered for an RBFN configuration are shown in Table.3.

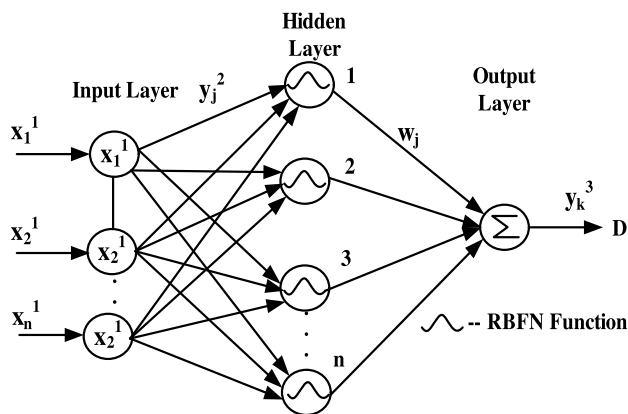


FIGURE 5. Control model of an RBFN.

TABLE 3. Parameter configuration of an RBFN

S.No	Controller parameters	Values/Methods
1	Input variables	$V_{A, B, C}$ and $I_{A, B, C}$
2	Output variables	D (Duty cycle)
3	Hidden neurons (Maximum limit)	617
4	Training algorithm	OLS (Ordinary Least Squares) method
5	Speed factor	0.03

A. INPUT LAYER

In this layer, the measured input variables are directly transmitted to next level through the nodes. The net input and output [12]–[14] is represented as,

$$net_i^1 = x_i^1(N) \tag{14}$$

$$y_i^1(N) = f_i^1(net_i^1(N)) = net_i^1(N), \tag{15}$$

Where, $i = 1, 2 \dots n$.

B. HIDDEN LAYER

In this, a Gaussian function is performed for each and every node i.e. an RBFN is used as a membership function. The net input and output for the hidden layer is [12]–[14] represented as,

$$net_j^2(N) = (X - M_j)^T \sum_j (X - M_j) \tag{16}$$

$$y_j^2(N) = f_j^2(net_j^2(N)) = Exp(net_j^2(N)), \tag{17}$$

$j = 1, 2 \dots 9$

Where Mean = $M_j = [m_{1j} \ m_{2j} \ \dots \ m_{ij}]^T$ and

$$\text{Standard deviation} = \sum_j = \text{diag}[\frac{1}{\sigma_{1j}^2} \ \frac{1}{\sigma_{2j}^2} \ \dots \ \frac{1}{\sigma_{ij}^2}]^T$$

C. OUTPUT LAYER

The overall output can be computed by the summation of all the inputs through the single node k, which is [12]–[14], represented as \sum , therefore

$$net_k^3 = \sum W_j y_j^2(N) \tag{18}$$

$$y_k^3(N) = f_k^3(net_k^3(N)) = net_k^3(N) = D \tag{19}$$

$$y_i^1(N) = f_i^1(net_i^1(N)) = net_i^1(N), \text{ where, } i = 1, 2 \tag{20}$$

In this controller configuration, the desired system operation is obtained by considering input data of 617 values of voltage and current from PMSG and the response of the RBFN controller has tuned automatically according to the change in the input parameters.

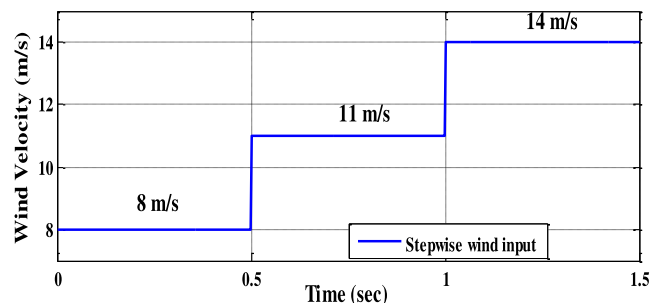


FIGURE 6. Different level of input wind velocity (m/s).

IV. SIMULATION RESULTS AND DISCUSSION

A. STANDALONE WIND ENERGY CONVERSION SYSTEM

In this research analysis, wind energy conversion system is designed for the standalone operation of an RBFN controller based Vienna Rectifier configuration. Stepwise wind velocity considered for the wind turbine is 8m/s (0 to 0.5s), 11m/s (0.5 to 1s) and 14m/s (1 to 1.5s) as shown in Figure 6. Design parameters considered for the simulation of Vienna rectifier are shown in Table 4. The output of the PMSG and Vienna Rectifier is changed with respect to the wind velocity. The output voltage, current, and power of the rectifier are depicted in Figure 7. Equal distribution of voltage across the DC-link

TABLE 4. Circuit parameters for the base speed (12m/s).

S.No	Circuit parameters	Ratings
1	Three phase input voltage	230V
2	Maximum output voltage of Vienna Rectifier	400V
3	Input inductance (L_i) ($L_A=L_B=L_C$)	10mH
4	Input filter capacitance (C_f) ($C_A=C_B=C_C$)	100uF
5	DC-link capacitance ($C_1 + C_2$)	200μF
6	Diode resistance (R_{ON})	0.001Ω
7	Load resistance (R)	160 Ω
8	Maximum output power	1kW

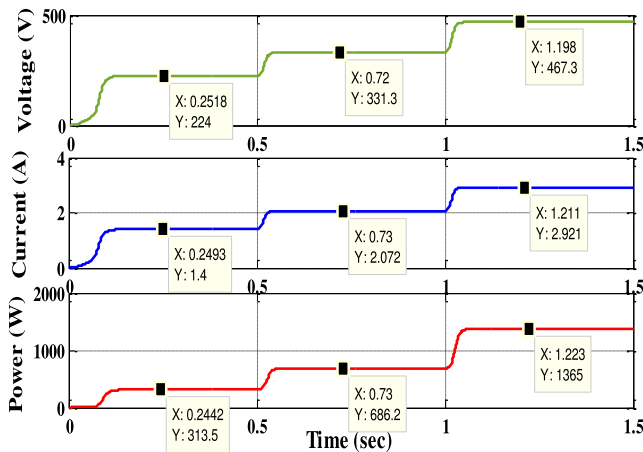


FIGURE 7. Output parameters of Vienna Rectifier for standalone system.

capacitors of Vienna Rectifier obtained in the standalone system is evident from Figure 8. It leads to balanced system configuration which ensures stable operation.

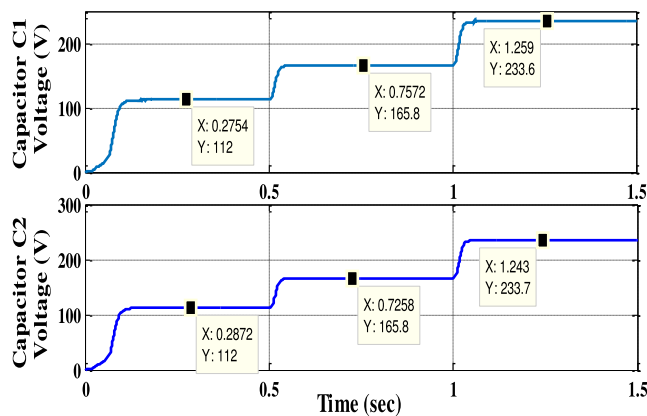


FIGURE 8. DC link voltage parameters of Vienna Rectifier for standalone system.

The output voltage of Vienna rectifier is obtained as 224V (0 to 0.5s), 331.3V (0.5 to 1s) and 467.3V (1 to 1.5s). Similarly, output current is obtained as 1.4A (0 to 0.5s),

2.072A (0.5 to 1s) and 2.921A (1 to 1.5s). Also, the output power of Vienna Rectifier is obtained as 313.5W for 0 sec to 0.5 sec, 686.2W for 0.5 to 1sec and 1365W for 1 to 1.5sec. The DC link capacitor voltages, 112V, 165.8V and 233.6V are equally distributed across the capacitors C_1 and C_2 in the circuit for the time intervals of 0 to 0.5s, 0.5 to 1s and 1 to 1.5s respectively. Complete result analysis of the Vienna rectifier is given in Table 5.

TABLE 5. Output parameters of an RBFN controller based vienna rectifier.

Parameters	Output values of an RBFN controller based Vienna Rectifier		
	0 to 0.5	0.5 to 1	1 to 1.5
Time Period (Sec)	0 to 0.5	0.5 to 1	1 to 1.5
Wind Velocity (m/s)	8	11	14
Voltage across capacitor C_1 (V)	112	168.8	233.6
Voltage across capacitor C_2 (V)	112	168.4	233.7
DC output voltage (V)	224	331.3	467.3
DC output current (A)	1.4	2.072	2.292
DC output power (W)	313.5	686.2	1365

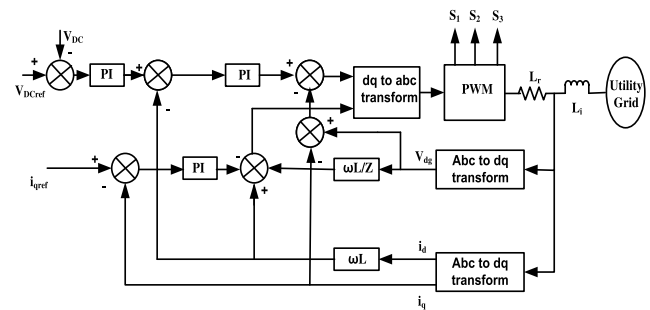


FIGURE 9. Block diagram of PWM controller of the grid side inverter.

B. GRID-TIED WIND ENERGY CONVERSION SYSTEM

In the grid-tied configuration, the DC-link has to be controlled to ensure constant voltage at the DC link. It results in balanced power between the DC link and utility grid. The grid side inverter controls the voltage and frequency as shown in Figure 9. Control variables i_d and i_q are used to control the active power and reactive power independently. The three-phase system (abc) is transformed [8], [24] into synchronous reference frame (dq) by the Park’s transformation. From the d -axis and q -axis control variables, the apparent power (S) can be [8], [24] written as,

$$S = (v_d i_d + v_q i_q) + j(v_q i_d - v_d i_q) \tag{21}$$

At Common Point of Interface (CPI), the d -axis voltage is considered as maximum and the q -axis voltage is considered as zero. Therefore the active power (P) & reactive power (Q) can be expressed as,

$$P = v_d i_d \tag{22}$$

$$Q = -v_d i_q \tag{23}$$

Where, v_d , i_d and v_q , i_q are the d -axis and q -axis voltage and current respectively. The negative sign of the equation 23

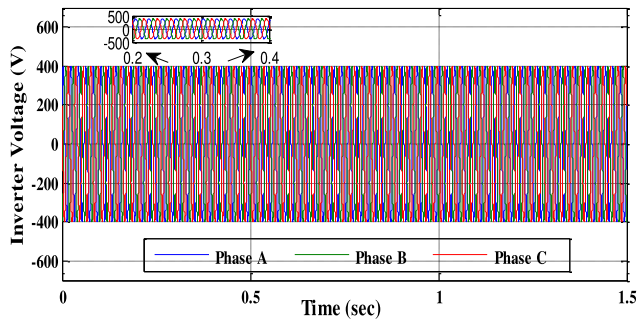


FIGURE 10. Inverter output voltage.

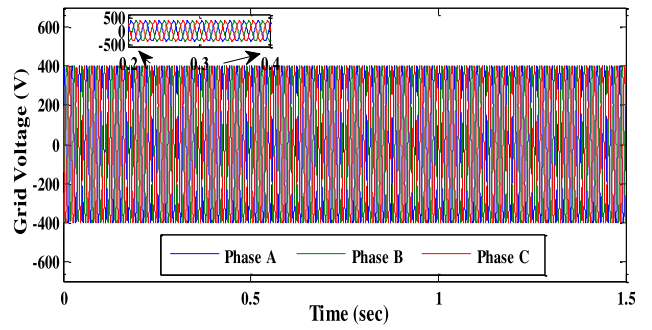


FIGURE 14. Grid output voltage.

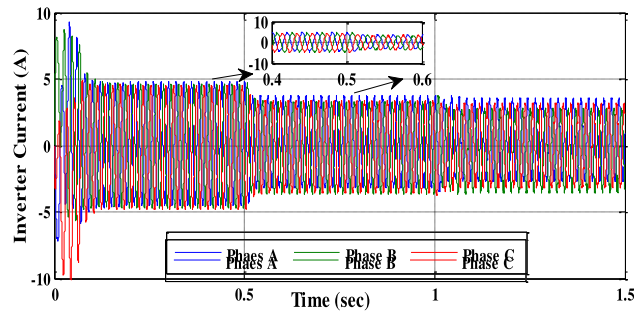


FIGURE 11. Inverter output current.

power and 900VAR reactive. The inverter, load, and grid side voltages and currents of three-phase grid-tied wind energy system are shown in Figure 10 to Figure 15.

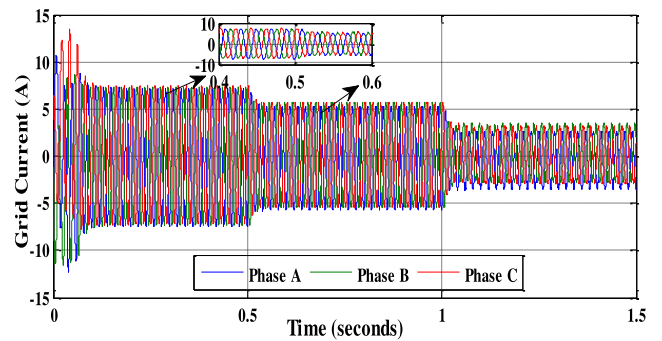


FIGURE 15. Grid output current.

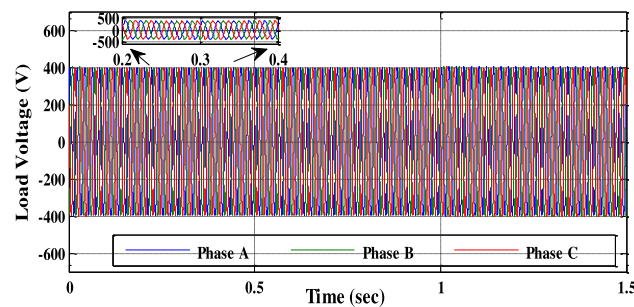


FIGURE 12. Load output voltage.

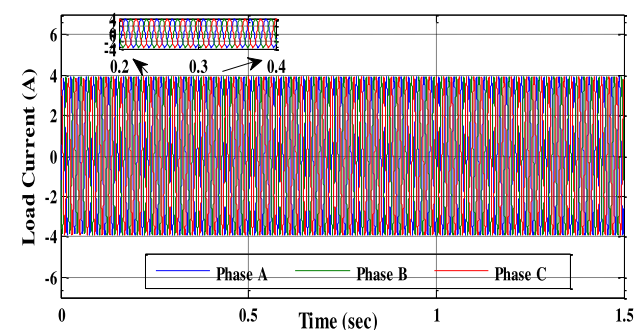


FIGURE 13. Load output current.

indicates that the exchange of reactive power is between the grid side inverter and the grid.

The grid-tied wind energy conversion system is validated in MATLAB Simulink software for a load of 1000W active

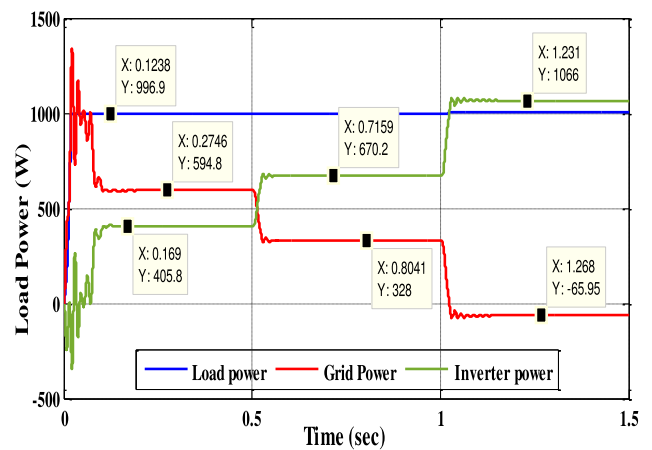


FIGURE 16. Active power output of the load, grid, and inverter in grid-tied system.

Figure 16 provides the inverter, load and grid side active power of grid-tied wind energy conversion system respectively. The load demand of 1000W for a period of 0 to 0.5s is supplied by both wind and grid sources (401.8W and 592.7W respectively). Similarly, during 0.5s to 1s, the load is supplied by both the wind and grid sources (670.3W and 328W respectively). For the period of 1s to 1.5s, power obtained from the

wind energy system is 1066 W which is more than the load demand (i.e. an excess of 65.95W wind-generated power is fed back to the grid).

Figure 17 gives the inverter, load and grid side reactive power profile of grid-tied wind energy system for the time intervals (0 to 0.5s, 0.5 to 1s and 1 to 1.5s respectively). From the above discussion, the developed wind energy system is able to meet the load demand by coordinating with the 400V, 50Hz AC grid system. Complete result analysis of active and reactive power supplied to load is given in Table 6.

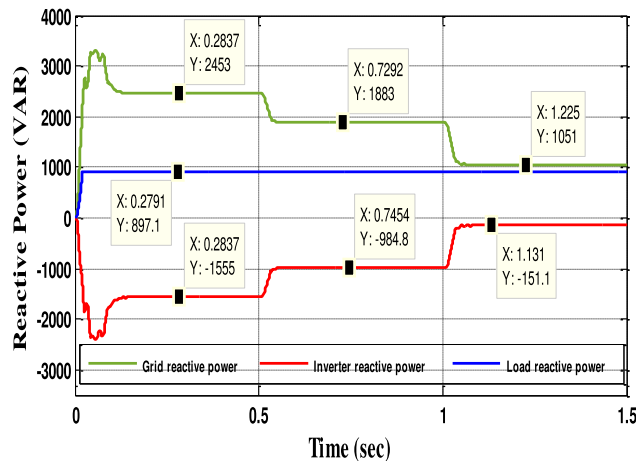


FIGURE 17. Reactive power output of the grid, inverter, and load in grid-tied system.

TABLE 6. Output parameters of inverter, grid and load.

Parameters	Active Power (W) =1000			Reactive Power (VAR) = 900			
	Time Period (Sec)	0 to 0.5	0.5 to 1	1 to 1.5	0 to 0.5	0.5 to 1	1 to 1.5
Inverter output		401.8	670.3	1066	-1555	-984.8	-151.1
Grid output		592.7	328	-65.94	2453	1883	1051
Load output		996.8	996.8	996.8	897.1	897.1	897.1

V. CONCLUSION

In this research, an RBFN controller based boost type Vienna rectifier has been implemented and simulated for grid-tied wind energy conversion system. The results of the proposed grid-tied wind energy system have been validated using MATLAB Simulink software for different input wind velocities under standalone and grid-tied conditions. In this proposed system, it has been proven that intelligent and dynamic controllers are suitable for controlling non-linear and complex systems. It is evident from detailed studies that the Vienna rectifier ensures AC/DC power conversion with improved power factor, reduced harmonics and sinusoidal input current wave shaping etc. This methodology of conversion is significant where unidirectional power flow (AC/DC) is necessary, especially in wind energy conversion systems,

data centers, telecommunication systems and DC distribution systems.

REFERENCES

- [1] N. Mendis, K. M. Muttaqi, S. Sayeef, and S. Perera, "Standalone operation of wind turbine-based variable speed generators with maximum power extraction capability," *IEEE Trans. Energy Convers.*, vol. 27, no. 4, pp. 822–834, Dec. 2012.
- [2] Y. Oğuz, İ. Güney, and H. Çalık, "Power quality control and design of power converter for variable-speed wind energy conversion system with permanent-magnet synchronous generator," *Sci. World J.*, vol. 2013, Sep. 2013, Art. no. 783010.
- [3] M. Benadja and A. Chandra, "A new MPPT algorithm for PMSG based grid connected wind energy system with power quality improvement features," in *Proc. IEEE 5th Power India Conf.*, Dec. 2012, pp. 1–6.
- [4] Y. Wang, J. Meng, X. Zhang, and L. Xu, "Control of PMSG-based wind turbines for system inertial response and power oscillation damping," *IEEE Trans. Sustain. Energy*, vol. 6, no. 2, pp. 565–574, Apr. 2015.
- [5] O. Alizadeh and A. Yazdani, "A strategy for real power control in a direct-drive PMSG-based wind energy conversion system," *IEEE Trans. Power Del.*, vol. 28, no. 3, pp. 1297–1305, Jul. 2013.
- [6] J. Chen, J. Chen, and C. Gong, "On optimizing the transient load of variable-speed wind energy conversion system during the MPP tracking process," *IEEE Trans. Ind. Electron.*, vol. 61, no. 9, pp. 4698–4706, Sep. 2014.
- [7] Z. Zhang, Y. Zhao, W. Qiao, and L. Qu, "A space-vector-modulated sensorless direct-torque control for direct-drive PMSG wind turbines," *IEEE Trans. Ind. Appl.*, vol. 50, no. 4, pp. 2331–2341, Jul./Aug. 2014.
- [8] X. Wang, S. Yuvarajan, and L. Fan, "MPPT control for a PMSG-based grid-tied wind generation system," in *Proc. IEEE North Amer. Power Symp. (NAPS)*, Sep. 2010, pp. 1–7.
- [9] Y. Xia, K. H. Ahmed, and B. W. Williams, "A new maximum power point tracking technique for permanent magnet synchronous generator based wind energy conversion system," *IEEE Trans. Power Electron.*, vol. 26, no. 12, pp. 3609–3620, Dec. 2011.
- [10] C. Wei, Z. Zhang, W. Qiao, and L. Qu, "An adaptive network-based reinforcement learning method for MPPT control of PMSG wind energy conversion systems," *IEEE Trans. Power Electron.*, vol. 31, no. 11, pp. 7837–7848, Nov. 2016.
- [11] R. Tiwari, S. Padmanaban, and R. B. Neelakandan, "Coordinated control strategies for a permanent magnet synchronous generator based wind energy conversion system," *Energies*, vol. 10, no. 10, p. 1493, Sep. 2017.
- [12] W. M. Lin, C.-M. Hong, T.-C. Ou, and T. M. Chiu, "Hybrid intelligent control of PMSG wind generation system using pitch angle control with RBFN," *Energy Convers. Manage.*, vol. 52, no. 2, pp. 1244–1251, Feb. 2011.
- [13] S. Saravanan and N. R. Babu, "RBFN based MPPT algorithm for PV system with high step up converter," *Energy Convers. Manage.*, vol. 122, pp. 239–251, Aug. 2016.
- [14] W.-M. Lin, C.-M. Hong, F.-S. Cheng, and K. H. Lu, "MPPT control strategy for wind energy conversion system based on RBF network," in *Proc. IEEE Energytech*, May 2011, pp. 1–6.
- [15] H. Chen, N. David, and D. C. Aliprantis, "Analysis of permanent-magnet synchronous generator with Vienna rectifier for wind energy conversion system," *IEEE Trans. Sustain. Energy*, vol. 4, no. 1, pp. 154–163, Jan. 2013.
- [16] X. Lu, Y. Xie, and L. Chen, "Feedback linearization and sliding mode control for VIENNA rectifier based on differential geometry theory," *Math. Problems Eng.*, vol. 2015, Sep. 2015, Art. no. 573016.
- [17] J. Adhikari, P. IV, G. Ponraj, and S. K. Panda, "Modeling, design, and implementation of a power conversion system for small-scale high-altitude wind power generating system," *IEEE Trans. Ind. Appl.*, vol. 53, no. 1, pp. 283–295, Jan./Feb. 2017.
- [18] J.-S. Lee and K.-B. Lee, "Performance analysis of carrier-based discontinuous PWM method for Vienna rectifiers with neutral-point voltage balance," *IEEE Trans. Power Electron.*, vol. 31, no. 6, pp. 4075–4084, Jun. 2016.
- [19] D. O. Boillat, F. Krismer, and J. W. Kolar, "EMI filter volume minimization of a three-phase, three-level T-type PWM converter system," *IEEE Trans. Power Electron.*, vol. 32, no. 4, pp. 2473–2480, Apr. 2017.
- [20] J.-S. Lee and K.-B. Lee, "A novel carrier-based PWM method for Vienna rectifier with a variable power factor," *IEEE Trans. Ind. Electron.*, vol. 63, no. 1, pp. 3–12, Jan. 2016.

- [21] J. Adhikari, P. IV, and S. K. Panda, "Reduction of input current harmonic distortions and balancing of output voltages of the Vienna rectifier under supply voltage disturbances," *IEEE Trans. Power Electron.*, vol. 32, no. 7, pp. 5802–5812, Jul. 2017.
- [22] B. Kedjar, H. Y. Kanaan, and K. Al-Haddad, "Vienna rectifier with power quality added function," *IEEE Trans. Ind. Electron.*, vol. 61, no. 8, pp. 3847–3856, Aug. 2014.
- [23] F. Flores-Bahamonde, H. Valderrama-Blavi, L. Martínez-Salamero, J. Maixé-Altés, and G. García, "Control of a three-phase AC/DC VIENNA converter based on the sliding mode loss-free resistor approach," *IET Power Electron.*, vol. 7, no. 5, pp. 1073–1082, Jan. 2014.
- [24] L. Hang, H. Zhang, S. Liu, X. Xie, C. Zhao, and S. Liu, "A novel control strategy based on natural frame for Vienna-type rectifier under light unbalanced-grid conditions," *IEEE Trans. Ind. Electron.*, vol. 62, no. 3, pp. 1353–1362, Mar. 2015.
- [25] J.-S. Lee and K.-B. Lee, "Carrier-based discontinuous PWM method for Vienna rectifiers," *IEEE Trans. Power Electron.*, vol. 30, no. 6, pp. 2896–2900, Jun. 2015.
- [26] M. Zhang, B. Li, L. Hang, L. M. Tolbert, and Z. Lu, "Performance study for high power density three-phase Vienna PFC rectifier by using SVPWM control method," in *Proc. IEEE 27th Annu. Appl. Power Electron. Conf. Expo. (APEC)*, Feb. 2012, pp. 1187–1191.
- [27] W. Yao, L. Zhengyu, M. Zhang, and Z. Lin, "A novel SVPWM scheme for Vienna rectifier without current distortion at current zero-crossing point," in *Proc. IEEE 23rd Int. Symp. Ind. Electron. (ISIE)*, Jun. 2014, pp. 2349–2353.
- [28] N. C. Foureaux, J. H. Oliveira, F. D. de Oliveira, B. de J. Cardoso Filho, and R. S. de Faria, "Command generation for wide-range operation of hysteresis-controlled Vienna rectifiers," *IEEE Trans. Ind. Appl.*, vol. 51, no. 3, pp. 2373–2380, May/Jun. 2015.
- [29] J.-S. Lee and K.-B. Lee, "Predictive control of Vienna rectifiers for PMSG systems," *IEEE Trans. Ind. Electron.*, vol. 64, no. 4, pp. 2580–2591, Apr. 2017.
- [30] K. Kumar, N. R. Babu, and K. R. Prabhu, "Design and analysis of RBFN-based single MPPT controller for hybrid solar and wind energy system," *IEEE Access*, vol. 5, pp. 15308–15317, 2017.
- [31] K.-W. Hu and C.-M. Liaw, "Development of a wind interior permanent-magnet synchronous generator-based microgrid and its operation control," *IEEE Trans. Power Electron.*, vol. 30, no. 9, pp. 4973–4985, Sep. 2015.
- [32] M. M. R. Singaravel and S. A. Daniel, "MPPT with single DC–DC converter and inverter for grid-connected hybrid wind-driven PMSG–PV system," *IEEE Trans. Ind. Electron.*, vol. 62, no. 8, pp. 4849–4857, Aug. 2015.



DAMODHAR REDDY was born in Mahbubnagar, India, in 1987. He received B.Tech. and M.Tech. degrees from JNTU Hyderabad in 2009 and 2013, respectively. He is currently pursuing the Ph.D. degree with VIT, Vellore. His research work interests in the field of power converters applications in the renewable energy systems, renewable energy resources, and hybrid microgrids.



SUDHA RAMASAMY was born in Salem, India, in 1974. She received the B.Sc. degree in industrial electronics from Bharathidasan University in 1995, the M.Sc. degree in applied electronics from Bharathiyar University in 1997, and the Ph.D. degree in electrical engineering from VIT, Vellore, in 2013. She is currently an Associate Professor with the School of Electrical Engineering, VIT. Her research interest is in renewable energy resources, sensors and signal conditioning, and low-cost biomedical devices.

• • •